PITM SIMULATIONS OF PASSIVE SCALAR TRANSPORT FIELDS IN TURBULENT FLOW AT LOW, MEDIUM AND HIGH PRANDTL NUMBERS

***B. Chaouat*[1] *and R. Schiestel*[2]**

[1] ***ONERA, Université Paris-Saclay, 92322 Chatillon, France***
[2] ***IRPHE/CNRS, 13384 Marseille, France***

Bruno.Chaouat@onera.fr

1 Introduction

Turbulent flows involving the transport of passive scalar are encountered in many fields of applications (Hanjalic and Launder, 2011) and are often simulated using different methods ranging from DNS, LES, RANS and RANS/LES (Chaouat, 2017). In this work, we consider the partially integrated transport modeling (PITM) method (Chaouat and Schiestel, 2005) using a second moment closure (SMC) that allows to perform simulations with seamless coupling between the RANS and LES regions and we extend this method to the case of passive scalar transport. We derive the basic transport equations for both the scalar variance of fluctuations k_θ and its dissipation-rate ϵ_θ in the spectral space (Chaouat and Schiestel, 2021). We perform then numerical simulations of turbulent channel flows including passive scalar fields on relatively coarse grids at the Reynolds number $R_\tau = 395$ for the Prandtl numbers $P_r = 0.1$, 1 and 10 associated with heat transfer of liquid metals, gas and water (see Fig 1). Comparison are made with DNS data (Chaouat and Peyret, 2019).

2 The basics of the PITM method for turbulent fields

From a physical standpoint, the PITM method finds its basic foundation in the spectral space of wave numbers considering the production, transfer and dissipation processes of energy acting in spectral wave number ranges of the spectrum. The starting point is the transport equation of the spherical mean of the Fourier transform of the two-point correlation tensor of the fluctuating velocities denoted $\varphi_{ij}(\boldsymbol{X}, \kappa, t)$ as follows (Chaouat and Schiestel, 2005; 2007; 2013)

$$\frac{\partial \varphi_{ij}(\boldsymbol{X},\kappa,t)}{\partial t} + \langle u_j \rangle (\boldsymbol{X}) \frac{\partial \varphi_{ij}(\boldsymbol{X},\kappa,t)}{\partial X_j} = \mathcal{P}_{ij}(\boldsymbol{X},\kappa,t) + \mathcal{T}_{ij}(\boldsymbol{X},\kappa,t) + \Psi_{ij}(\boldsymbol{X},\kappa,t) + \mathcal{J}_{ij}(\boldsymbol{X},\kappa,t) - \mathcal{E}_{ij}(\boldsymbol{X},\kappa,t) \quad (1)$$

where $\mathcal{P}_{ij}$, $\mathcal{T}_{ij}$, Ψ_{ij}, $\mathcal{J}_{ij}$, and $\mathcal{E}_{ij}$ are respectively, the production, transfer, redistribution, diffusion and dissipation terms, the brackets $\langle . \rangle$ denotes the averaging in homogeneous directions of the flow. The PITM equations are then formally obtained from integration of Equation (1) in the wave number ranges $[0, \kappa_c]$, $[\kappa_c, \kappa_d]$ and $[\kappa_d, \infty[$, where κ_c is the cutoff wave number linked to the filter size Δ by $\kappa_c = \pi/\Delta$, and κ_d is the dissipative wave number located at the far end of the inertial range of the spectrum. As a result (Schiestel and Dejoan, 2005; Chaouat and Schiestel, 2005, 2009, 2012), the transport equation for the subfilter scale stress (SFS) tensor $(\tau_{ij})_s$ can be written in the simple compact form as

$$\frac{\partial (\tau_{ij})_s}{\partial t} + \frac{\partial}{\partial x_k}(\bar{u}_k (\tau_{ij})_s) = (P_{ij})_s + (\Pi_{ij})_s - \epsilon_{ij} + (J_{ij})_s \quad (2)$$

where the terms appearing in the right-hand side of this equation are identified as subfilter production, redistribution and dissipation, respectively while the transport equation for the dissipation rate ϵ can be expressed into the form

$$\frac{\partial \epsilon}{\partial t} + \frac{\partial}{\partial x_k}(\bar{u}_k \epsilon) = c_{\epsilon 1 s} \frac{\epsilon}{k_s} P_s - c_{\epsilon 2 s} \frac{\epsilon^2}{k_s} + J_{\epsilon s} \quad (3)$$

the bar $\bar{.}$ denotes the filtering. The coefficient appearing in the destruction term of Equation (3) is

then given by

$$c_{\epsilon_{2s}} = c_{\epsilon_1} + \frac{k_s}{k}\Delta c_\epsilon \tag{4}$$

where $\Delta c_\epsilon = c_{\epsilon 2} - c_{\epsilon 1}$, c_{ϵ_1} and c_{ϵ_2} are the coefficients used in RANS and $c_{\epsilon 1s} = c_{\epsilon_1}$. Using an equilibrium density spectrum defined as $E(\kappa) = kLE^*(\vartheta)$, where L denotes the turbulence length-scale $L = k^{3/2}/\epsilon$, $\vartheta = \kappa L$,

$$E^*(\vartheta) = \frac{\frac{2}{3}\beta\vartheta^{\alpha-1}}{[1+\beta\vartheta^\alpha]^{\gamma+1}} \tag{5}$$

one can obtain after integration

$$c_{\epsilon_{2s}} = c_{\epsilon_1} + \frac{\Delta c_\epsilon}{[1+\beta\vartheta_c^\alpha]^\gamma} \tag{6}$$

where $\alpha\gamma = 2/3$ and $\beta = [2/(3C_K)]^\gamma$, C_K is the Kolmogorov constant close to 1.5, $\vartheta_c = \kappa_c L$,

Turbulent passive scalar field. We extend here the PITM method developed for dynamic turbulent fields to scalar fields. As for the preceding section, the key is to work in the spectral space. The spectral transport equation of half the scalar variance denoted as $E_\theta(\boldsymbol{X},\kappa) = \langle\theta'\theta'(\boldsymbol{X})\rangle^\Delta(\kappa)/2$ reads (Chaouat and Schiestel, 2021)

$$\begin{aligned}&\frac{\partial E_\theta(\boldsymbol{X},\kappa)}{\partial t} + \langle u_k\rangle(\boldsymbol{X})\frac{\partial E_\theta(\boldsymbol{X},\kappa)}{\partial X_k}\\ &= \mathcal{P}_\theta(\boldsymbol{X},\kappa) + \mathcal{T}_\theta(\boldsymbol{X},\kappa) + \mathcal{J}_\theta(\boldsymbol{X},\kappa)\\ &-\mathcal{E}_\theta(\boldsymbol{X},\kappa)\end{aligned} \tag{7}$$

where in the right hand side of this equation, $\mathcal{P}_\theta$ is the production of half the scalar variance by mean gradients of the scalar, $\mathcal{T}_\theta$ is the spectral transfer driven by the eddying motions in the inertial cascade, $\mathcal{J}_\theta$ is the diffusion term and $\mathcal{E}_\theta$ denotes the dissipation term of half the scalar variance. Equation (7) is integrated in the domains $[0,\kappa_c]$, $[\kappa_c,\kappa_e]$ and $[\kappa_e,\infty[$ where κ_e denotes here the high end wave number for the scalar that is larger than κ_c and different from κ_d. Homogeneous flows are considered in the following. As a result, the transport equation for the subfilter scale variance $k_{\theta s}$ can be written formally as

$$\frac{\partial k_{\theta s}}{\partial t} = P_{\theta[\kappa_c,\kappa_e]} + F_\theta(\kappa_c,t) - \epsilon_\theta \tag{8}$$

where the total variance transfer $F_\theta(\kappa_e,t)$ through the variable cutoff κ_e is defined as

$$F_\theta(\kappa_c,t) = \mathcal{F}_\theta(\kappa_c,t) - E_\theta(\kappa_c,t)\frac{\partial\kappa_c}{\partial t} \tag{9}$$

that takes into account the local spectral flux $\mathcal{F}_\theta(\kappa_c,t)$ and the transfer due to the variation in the splitting wavenumber and

$$F_\theta(\kappa_e,t) = \mathcal{F}_\theta(\kappa_e,t) - E_\theta(\kappa_e,t)\frac{\partial\kappa_e}{\partial t} \tag{10}$$

The relation $\kappa_e - \kappa_c = \mathcal{O}(1/l_\theta) = \mathcal{O}(\epsilon_\theta/\theta^2 u)$ leads to the equation

$$\kappa_e - \kappa_c = \zeta_\theta\frac{\epsilon_\theta}{k_{\theta s}k_s^{1/2}} \tag{11}$$

where ζ_θ is an adjustable coefficient chosen such that the spectral contribution of the variance beyond κ_e is negligible. Combining these equations together yields in homogeneous flows

$$\begin{aligned}\frac{\partial\epsilon_\theta}{\partial t} &= \frac{\epsilon_\theta}{k_{\theta s}}\frac{\partial k_{\theta s}}{\partial t} + \frac{\epsilon_\theta}{2k_s}\frac{\partial k_s}{\partial t}\\ &+\frac{\epsilon_\theta}{\kappa_e-\kappa_c}\left[\frac{\mathcal{F}_\theta(\kappa_e,t)-F_\theta(\kappa_e,t)}{E_\theta(\kappa_e,t)}\right]\\ &-\frac{\epsilon_\theta}{\kappa_e-\kappa_c}\left[\frac{\mathcal{F}_\theta(\kappa_c,t)-F_\theta(\kappa_c,t)}{E_\theta(\kappa_c,t)}\right]\end{aligned} \tag{12}$$

Using the transport equations for k_s and Equation (3), one can obtain the resulting equation for the dissipation-rate ϵ_θ written in a more general form as

$$\begin{aligned}\frac{\partial\epsilon_\theta}{\partial t} &= c_{\epsilon_{\theta\theta_{1s}}}P_{\theta s}\frac{\epsilon_\theta}{k_{\theta s}} + c_{\epsilon_{\theta k_{1s}}}P_s\frac{\epsilon_\theta}{k_s} - c_{\epsilon_{\theta k_{2s}}}\frac{\epsilon_\theta\epsilon}{k_s}\\ &-c_{\epsilon_{\theta\theta_{2s}}}\frac{\epsilon_\theta^2}{k_{\theta s}}\end{aligned} \tag{13}$$

where

$$P_{\theta s} = P_{\theta[\kappa_c,\kappa_e]} + F_\theta(\kappa_c) \tag{14}$$

$c_{\epsilon_{\theta\theta_{1s}}} = 1$, $c_{\epsilon_{\theta k_{1s}}} = 1/2$, $c_{\epsilon_{\theta k_{2s}}} = 1/2$,

$$c_{\epsilon_{\theta\theta_{2s}}} = 1 - \frac{k_{\theta s}}{\kappa_e E_\theta(\kappa_e)}\left(\frac{\mathcal{F}_\theta(\kappa_e)}{\epsilon_\theta} - 1\right) \tag{15}$$

assuming that $\kappa_c \ll \kappa_e$, $E(\kappa_d) \ll E(\kappa_c)$, and $E_\theta(\kappa_e) \ll E_\theta(\kappa_c)$, and also considering that $F_\theta(\kappa_e) = \epsilon_\theta$. When κ_c goes to zero, that is to say when the filter width in physical space goes to infinity in an homogeneous turbulence field (or locally homogeneous), one recovers the equation used in statistical RANS closure. Hence, the equation can be written as

$$\begin{aligned}\frac{\partial\epsilon_\theta}{\partial t} &= c_{\epsilon_{\theta\theta_1}}P_\theta\frac{\epsilon_\theta}{k_\theta} + c_{\epsilon_{\theta k_1}}P\frac{\epsilon_\theta}{k} - c_{\epsilon_{\theta k_2}}\frac{\epsilon_\theta\epsilon}{k}\\ &-c_{\epsilon_{\theta\theta_2}}\frac{\epsilon_\theta^2}{k_\theta}\end{aligned} \tag{16}$$

where $c_{\epsilon_{\theta\theta_1}} = 1$, $c_{\epsilon_{\theta k_1}} = 1/2$, $c_{\epsilon_{\theta k_2}} = 1/2$,

$$c_{\epsilon_{\theta\theta_2}} = 1 - \frac{k_\theta}{\kappa_e E_\theta(\kappa_e)} \left(\frac{\mathcal{F}_\theta(\kappa_e)}{\epsilon_\theta} - 1 \right) \quad (17)$$

The final transport equations for the subfilter scalar variance k_{θ_s} and its dissipation-rate ϵ_θ including the convection and diffusion terms read

$$\frac{\partial k_{\theta s}}{\partial t} + \frac{\partial}{\partial x_k}(\bar{u}_k k_{\theta s}) = P_{\theta s} - \epsilon_\theta + J_{\theta s} \quad (18)$$

$$\frac{\partial \epsilon_\theta}{\partial t} + \frac{\partial}{\partial x_k}(\bar{u}_k \epsilon_\theta) = c_{\epsilon_{\theta\theta_1}} P_{\theta s} \frac{\epsilon_\theta}{k_{\theta s}} + c_{\epsilon_{\theta k_1}} P_s \frac{\epsilon_\theta}{k_s} - c_{\epsilon_{\theta k_2}} \frac{\epsilon_\theta \epsilon}{k_s} - c_{\epsilon_{\theta\theta_2 s}} \frac{\epsilon_\theta^2}{k_{\theta s}} + J_{\epsilon_{\theta s}} \quad (19)$$

where $c_{\epsilon_{\theta\theta_1}}$, $c_{\epsilon_{\theta k_1}}$, $c_{\epsilon_{\theta k_2}}$ are constant coefficients whereas $c_{\epsilon_{\theta\theta_2 s}}$, combining Equations (15) and (17), is now a dynamical coefficient given by

$$c_{\epsilon_{\theta\theta_2 s}} = c_{\epsilon_{\theta\theta_1}} + \frac{k_{\theta s}}{k_\theta} \Delta c_{\epsilon_{\theta\theta}} \quad (20)$$

where $\Delta c_{\epsilon_{\theta\theta}} = c_{\epsilon_{\theta\theta_2}} - c_{\epsilon_{\theta\theta_1}}$. The variance ratio in Equation (20) is computed considering different spectra $E_\theta(\kappa)$ of the passive scalar associated with small, medium and high Prandtl number.

Molecular Prandtl numbers near unity

The ratio $k_{\theta s}/k_\theta$ appearing in Equation (20) is computed using the spectrum of the scalar in the equilibrium range can be approximated by

$$E_\theta(\kappa) = C_\theta \epsilon_\theta \epsilon^{-1/3} \kappa^{-5/3} \quad (21)$$

where C_θ is a constant coefficient close to 0.5. The spectrum of the scalar θ given by Eq. (21) is extended in the whole range domain of the wavenumbers as

$$E_\theta(\kappa) = \frac{C_\theta \epsilon_\theta}{C_K \epsilon} E(\kappa) \quad (22)$$

using the spectrum $E(\kappa) = kLE^*(\vartheta)$ where $E^*(\vartheta)$ is given by Equation (5). The analytical integration yields the practical result given by Equation (A1) that is analogous to the formula previously obtained for the dynamical equations for kinetic energy.

Small molecular Prandtl numbers

This situation corresponds to the case of liquid metals. The inertial subrange of the variance spectrum is shorter due to high molecular diffusivity. The spectrum of the scalar variance is given by the function

$$E_\theta(\kappa) = C_\theta \epsilon_\theta \epsilon^{-1/3} \kappa^{-5/3} \exp\left[-\frac{3}{2} C_\theta (\kappa \eta_\theta)^{4/3} \right] \quad (23)$$

with the scalar microscale defined by $\eta_\theta = \left(\sigma^3/\epsilon\right)^{1/4}$ where $C_\theta = 1.5$. Using the Kolmorogov scale $\eta_K = (\nu^3/\epsilon)^{1/4}$ and the Prandtl number $P_r = \nu/\sigma$, the scalar microscale can be computed by $\eta_\theta = \eta_K / P_r^{3/4}$. In practice, Equation (23) is replaced by

$$E_\theta(\kappa) = C_\theta \epsilon_\theta \epsilon^{-1/3} \kappa^{-5/3} H(\kappa_H - \kappa) \quad (24)$$

where $\kappa_H = 1/\eta_\theta$, and H is the Heaviside function implying that $E_\theta(\kappa) = 0$ for $\kappa \geq \kappa_H$. The spectral vanishing value of wavenumber is then obtained for $\kappa \eta_\theta = 1$. So that the dimensionless variable ϑ is dropping for $\vartheta_H = (P_r Re_t)^{3/4}$ where $Re_t = k^2/\nu\epsilon$ denotes the turbulent Reynolds number. This dropping value can be expressed equivalently as $\vartheta_H = k^{3/2}/(\eta_\theta\, \epsilon) = (\sigma k^2/\epsilon)^{3/4}$. Physically, the dimensionless group $P_r Re_t$ is interpreted like the turbulent Peclet number denoted $Pe_t = P_r Re_t$. The exact final expression of the coefficient $c_{\epsilon_{\theta\theta_2 s}}$ is obtain by integrating the spectrum (24) leading to Equation (A2).

Large molecular Prandtl numbers

This situation corresponds to the case of poorly conducting fluids or high viscous fluids like most of oils. The inertial subrange is followed by a viscous-convective subrange with a negative slope of minus unity and a viscous-diffusive subrange in which the spectrum undergoes strong decay. For the wave number $\kappa \geq 1/\eta_K$, it can be shown that the viscous convective subrange of the spectrum is of the form

$$E_\theta(\kappa) = c_\theta \epsilon_\theta \left(\frac{\nu}{\epsilon} \right)^{1/2} \kappa^{-1} \quad (25)$$

where c_θ is a constant coefficient. The viscous convective subrange is followed by the viscous-diffusive subrange which is characterized by the role of scalar diffusivity acting on very small scales. In this region, the spectrum takes on the form

$$E_\theta(\kappa) = c_\theta \epsilon_\theta \left(\frac{\nu}{\epsilon} \right)^{1/2} \kappa^{-1} \exp\left[-c_\theta (\kappa \eta_\theta^*)^2 \right] \quad (26)$$

where $\eta_\theta^* = \eta_K (\sigma/\nu)^{1/2} = \eta_K/\sqrt{P_r}$ is the smallest scale of the viscous-diffusive subrange

and c_θ is a constant coefficient. The corresponding wave numbers are then computed as $\kappa_K = 1/\eta_K$ and $\kappa_S = 1/\eta_\theta^*$. The junctions between the different curves occur for $\kappa = \kappa_K$ and $\kappa = \kappa_S$, respectively. In particular, for $\kappa = \kappa_K$, the spectrum $E_\theta(\kappa_K)$ given by Equation (21) of the scalar in the equilibrium range with a slope $\kappa^{-5/3}$ is equal to the spectrum $E_\theta(\kappa_K)$ given by Equation (25) of the viscous-convective subrange with a slope κ^{-1}, so that $c_\theta = C_\theta \approx 1.5$. The dimensionless wave numbers $\vartheta = \kappa L$ associated with the Kolmogorov scale η_K and the smallest scale η_θ^* are $\vartheta_K = Re_t^{3/4}$ and $\vartheta_S = P_r^{1/2} Re_t^{3/4}$, respectively. In practice, a simple approach is retained. The spectrum given by Equation (26) is replaced by a simple form as

$$E_\theta(\kappa) = c_\theta \epsilon_\theta \left(\frac{\nu}{\epsilon}\right)^{1/2} \kappa^{-1} H(\kappa_S - \kappa) \qquad (27)$$

implying that $E_\theta(\kappa) = 0$ for $\kappa \geq \kappa_S$. The wave number range $[0, \kappa_S]$ is then decomposed into two wave number ranges introducing the cutoff wave number κ_c where $\kappa_c < \kappa_S$ or $\kappa_c > \kappa_S$. In the first wave number range $[0, \kappa_K]$, the spectrum $E_{\theta_1}(\kappa)$ is defined as

$$E_{\theta_1}(\kappa) = \xi \frac{k_\theta}{k} E(\kappa) \qquad (28)$$

where $E(\kappa)$ is given by Equation (5) whereas in the second domain $[\kappa_K, \infty[$, the spectrum $E_{\theta_2}(\kappa)$ is deduced from Equation (27)

$$E_{\theta_2}(\kappa) = \xi c_\theta \epsilon_\theta \left(\frac{\nu}{\epsilon}\right)^{1/2} \kappa^{-1} H(\kappa_S - \kappa) \qquad (29)$$

where ξ is a coefficient of normalization. An analytical integration provides the exact expression of the $c_{\epsilon_{\theta\theta_2 s}}$ coefficient given in Equation (A3).

3 PITM simulation of the channel flow heated on both walls

As a generic test case, the fully developed turbulent channel flow heated on both walls is simulated. The variable θ is normalized by the surface scalar flux defined as $\theta_\tau = q_w/(\rho c_p u_\tau)$ where ρ, c_p and q_w are the fluid density, the specific heat at constant pressure and the heat flux at the wall. The heat flux is given by $q_w = -\lambda(\partial\theta/\partial x_3)_w$ where λ stands for the thermal conductivity $\lambda = \rho c_p \nu / P_r$.

Case $P_r \approx 1$

$$c_{\epsilon_{\theta\theta_2 s}} = c_{\epsilon_{\theta\theta_1}} + \Delta c_{\epsilon_{\theta\theta}} . \mathcal{G} \qquad (A1)$$

with $\mathcal{G} = [1 + \beta \vartheta_c^\alpha]^{-\gamma}$ and $\alpha\gamma = 2/3$ in practice $\alpha = 3$, $\gamma = 2/9$ and $\beta = (3C_K/2)^{-\gamma}$

Case $P_r \ll 1$

$$c_{\epsilon_{\theta\theta_2 s}} = \begin{cases} c_{\epsilon_{\theta\theta_1}} + \Delta c_{\epsilon_{\theta\theta}} \dfrac{\mathcal{G} - \mathcal{H}}{1 - \mathcal{H}} & (\vartheta_c < \vartheta_H) \\ c_{\epsilon_{\theta\theta_1}} & (\vartheta_c > \vartheta_H) \end{cases} \qquad (A2)$$

with $\mathcal{H} = \left[1 + \beta Pe_t^{3\alpha/4}\right]^{-\gamma}$

Case $P_r \gg 1$

$$c_{\epsilon_{\theta\theta_2 s}} = \begin{cases} c_{\epsilon_{\theta\theta_1}} + \Delta c_{\epsilon_{\theta\theta}} \dfrac{\mathcal{G} - \mathcal{S} + \mathcal{Z}}{1 - \mathcal{S} + \mathcal{Z}} & (\vartheta_C < \vartheta_K) \\ c_{\epsilon_{\theta\theta_1}} + \Delta c_{\epsilon_{\theta\theta}} \dfrac{c_\theta \frac{\epsilon_\theta}{k_\theta} \left(\frac{\nu}{\epsilon}\right)^{1/2} \ln \frac{\vartheta_S}{\vartheta_c}}{1 - \mathcal{S} + \mathcal{Z}} & (\vartheta_K < \vartheta_C < \vartheta_S) \\ c_{\epsilon_{\theta\theta_1}} & (\vartheta_S < \vartheta_C) \end{cases} \qquad (A3)$$

with $\mathcal{S} = \left[1 + \beta Re_t^{3\alpha/4}\right]^{-\gamma}$ and $\mathcal{Z} = c_\theta \frac{\epsilon_\theta}{k_\theta} \left(\frac{\nu}{\epsilon}\right)^{1/2} \ln P_r^{1/2}$

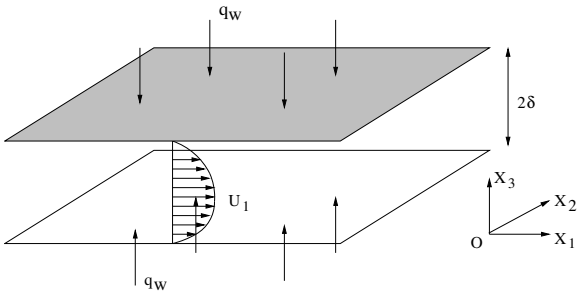

Figure 1: Setup of the numerical channel flow simulations subjected to heat fluxes.

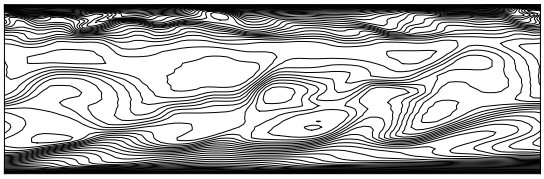

Figure 2: Contours of the instantaneous passive scalar in the (x_1, x_3) mid-plane illustrating the unsteady character of the scalar field. $P_r = 1$.

Numerical procedure

The dimension of the channel in the streamwise, spanwise and normal directions along the axes x_1, x_2, x_3 are $L_1 = 6.4\delta$, $L_2 = 3.2\delta$ and $L_3 = 2\delta$. The grid resolutions are $84 \times 42 \times 84$ for $P_r = 0.1$, 1 and $84 \times 42 \times 128$ for $P_r = 10$, respectively. The mesh is uniform in the streamwise and spanwise directions, $\Delta_1^+ = \Delta_2^+ = 30$, while in the direction x_3, the grid is refined near the walls. The Batchelor length-scale is given by $\eta_\theta = \eta_K / P_r^{3/4} \approx 5.62\,\eta_K$ at $P_r = 0.1$, $\eta_\theta \approx \eta_K$ at $P_r = 1$, and $\eta_\theta = \eta_K / P_r^{1/2} \approx 0.316\,\eta_K$ at $P_r = 10$. The simulations are performed using the numerical code (Chaouat, 2011) which is based on the finite volume technique with MPI.

4 Numerical results

The transformed variable $\Theta^+ = \theta_w^+ - \theta^+$ is considered to analyze the results. Comparions are made with DNS (Chaouat and Peyret, 2019). Figure 2 shows the contours plots of the instantaneous scalar field for the Prandtl number $P_r = 1$ in the mid-plane of the channel illustrating the detachment of vortex in the normal direction. Fig. 3 shows the mean scalar variable Θ^+ versus the logarithmic wall distance. It is found that the PITM velocity profile present an excellent agreement with the DNS data at each Prandtl number although the grid is coarse. Fig. 4 displays the *rms* scalar variance θ_{rms} and indicates a good agreement with the reference data. The distribution of the subgrid scale fluctuations relatively to the resolved scale fluctuations is governed by the wave numbers appearing in the spectrum partition E_θ with influence of Prandtl number.

5 Conclusion

As a result of physical modeling in the spectral space of wave numbers, the subfilter PITM model has been extended for accounting of heat transfer in hybrid RANS/LES simulations. Numerical simulations of the turbulent channel flow with scalar fields have been then performed on coarse grids at $R_\tau = 395$ for $P_r = 0.1$, 1 and 10. The distributions of the mean scalar variable $\langle\theta\rangle$ and *rms* scalar fluctuations $\theta_{rms} = \langle\theta'\theta'\rangle$ were fairly well predicted.

References

Chaouat, B. and Schiestel, R. (2005). A new partially integrated transport model for subgrid-scale stresses and dissipation rate for turbulent developing flows, Phys. Fluids, **17**, 065106, 1-19.

Chaouat, B. and Schiestel, R. (2007). From single-scale turbulence models to multiple-scale and subgrid-scale models by Fourier transform, Theor. Comput. Fluid Dyn, **21**, 201-229.

Chaouat, B. (2011). An efficient numerical method for RANS/LES turbulent simulations using subfilter scale stress transport equations, Int. J. Numer. Methods Fluids 67, 1207-1233.

Chaouat, B. and Schiestel, R. (2013). Partially integrated transport modeling method for turbulence simulation with variable filters, Phys. Fluids, **25**, 125102, 1-39.

Chaouat, B. (2017). The state of the art of hybrid RANS/LES modeling for the simulation of turbulent flows. Flow, Turbul. Combust., 99, 279-327.

Chaouat, B. and Peyret, C. (2019). Investigation of the wall scalar fluctuations effect on passive scalar turbulent fields at several Prandtl numbers by means of direct numerical simulations, J. Heat Transfer, ASME, **141**, 1-12.

Chaouat, B., Schiestel, R. (2021). Extension of the partially integrated transport modeling method to the simulation of passive scalar turbulent fluctuations at various Prandtl numbers. Int. J. Heat Fluid Flow, **89**, 1-19.

Hanjalic, K. and Launder, B.E. (2011). Modelling turbulence in engineering and the environment. Second-moment route to closure, Cambridge University Press.

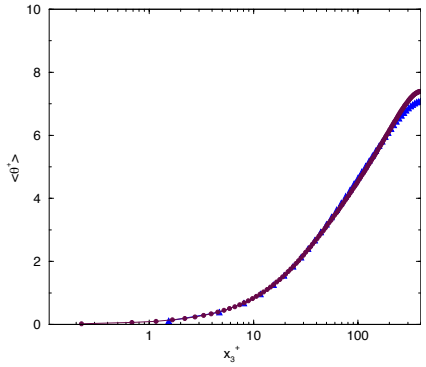

(a)

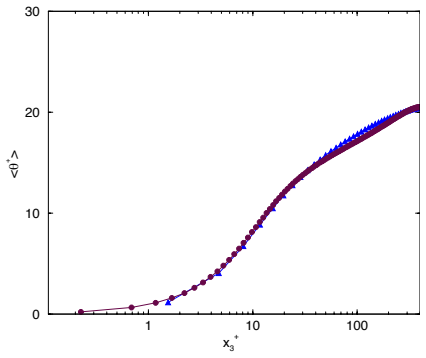

(b)

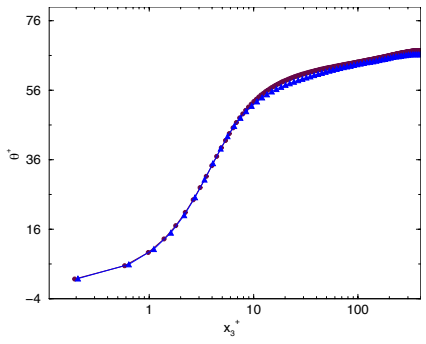

(c)

Figure 3: Mean scalar field $\langle \theta^+ \rangle$ in logarithmic coordinate versus the wall unit distance for several P_r numbers. DNS : •; PITM : ▲. (a) $P_r = 0.1$; (b) $P_r = 1$; (c) $P_r = 10$; $R_\tau = 395$.

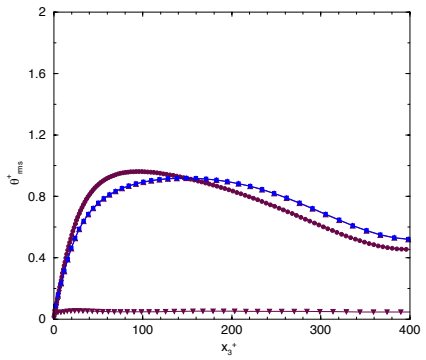

(a)

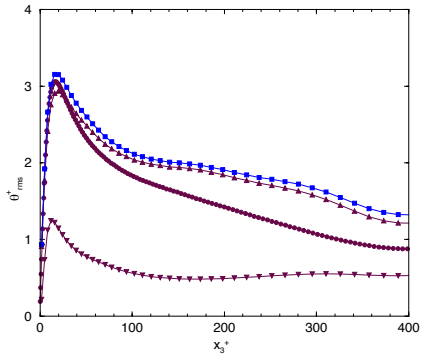

(b)

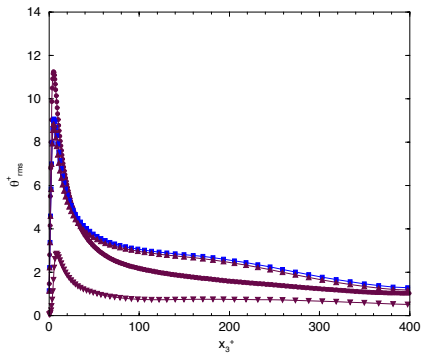

(c)

Figure 4: Root mean square of the scalar variance $\theta^+_{rms} = \sqrt{\langle \theta'^+ \theta'^+ \rangle}$ versus the wall distance for several P_r numbers. DNS : •; PITM : ■. Subgrid scale : ▼; Resolved scale : ▲. (a) $P_r = 0.1$; (b) $P_r = 1$; (c) $P_r = 10$; $R_\tau = 395$.